

Tensile Properties of Friction Stir Welds of AA 7020 Aluminum Alloy

Akbar Heidarzadeh · Reza Vatankhah Barenji ·
Mohsen Esmaily · Atabak Rahimzadeh Ilkhichi

Received: 15 October 2014 / Accepted: 24 December 2014 / Published online: 1 March 2015
© The Indian Institute of Metals - IIM 2015

Abstract In this investigation, response surface methodology was used to predict and optimize the tensile properties of friction stir welded AA 7020 aluminum alloy. Tensile properties, microstructural features and fractography of the joints were measured and investigated using tensile test, optical and scanning electron microscopes, respectively. In addition, the influences of friction stir welding parameters on tensile properties of the joints were examined thoroughly. The results revealed that with increasing the heat input, the tensile strength of the joints increased up to a maximum value and then decreased, where the elongation of the joints increased continuously. Moreover, the optimal condition to obtain a maximum of tensile strength was 1,055 rpm, 97 mm/min and 7.4 kN, where as for tensile elongation was 1,320 rpm, 72 mm/min and 7 kN.

Keywords Friction stir welding · Tensile strength · Elongation · Modeling

A. Heidarzadeh (✉)
Young Researchers and Elite Club, Ahar Branch, Islamic Azad University, Ahar, Iran
e-mail: ak.hz62@gmail.com

R. V. Barenji
Department of Industrial Engineering, Hacettepe University, Beytepe Campus, Ankara, Turkey

M. Esmaily
Department of Chemical and Biological Engineering, Chalmers University of Technology, 412 96 Gothenburg, Sweden

A. R. Ilkhichi
Department of Mechanical Engineering, Eastern Mediterranean University, Famagusta, Mersin, Turkey

1 Introduction

Friction stir welding (FSW) was invented at The Welding Institute of UK in 1991 and was originally conducted for joining the aluminum alloys [1]. FSW is a solid state process which eliminates the conventional fusion welding defects such as large distortion, large heat affected zone (HAZ), solidification cracking, porosity, oxidation, and etc. [2]. Therefore, joints produced using FSW show better mechanical properties such as the ultimate tensile strength (UTS), tensile elongation (EI), and hardness in comparison with the joints welded by fusion methods. Consequently, these advantages of the FSW have made it an excellent candidate for joining a variety of different metals and alloys, in recent years [3–6].

The mechanical properties of the joints welded by all types of welding methods play an important role in their industrial performance. Furthermore, in the case of FSW, the mechanical features of the joints are generally influenced by FSW parameters such as tool rotational speed, welding speed, tool pin profile, axial force, etc., which should be optimized to reach the best mechanical properties. Response Surface Methodology (RSM) was invented by Box and Wilson [7] in 1951, and it has been used to model and optimize the FSW process [8–21]. The RSM has two main aims. The first one is optimizing the responses which are a function of various input parameters. The second one is predicting the mathematical relationships between the process parameters and the measured responses [22, 23]. The RSM include following steps for FSW process [24, 25]: Identifying the FSW parameters which have effect on mechanical properties of the joints; Considering reasonable limits of the identified parameters; Developing a desired experimental design; Performing the tests according to the developed experimental design; Measuring the responses; Establishing the mathematical models; Controlling the model adequacy using analysis of variance (ANOVA), and

exploring the influence of the parameters on responses and optimizing them.

Recently, some researchers have used RSM to predict or optimize the properties of friction stir welded joints of different metals and alloys [8–21]. For instance, Rajakumar et al. [9, 10] developed mathematical relationships to predict grain size, ultimate tensile strength (UTS) and hardness of friction stir welded AA 6061-T6 aluminium alloy joints using RSM. They showed that rotational speed of 1,100 rpm, welding speed of 80 mm/min, axial force of 8 kN, shoulder diameter of 15 mm, pin diameter of 5 mm and tool hardness

of 45 HRC, caused to highest mechanical properties. Similarly, Babu et al. [16] made an attempt to develop a mathematical model to predict the tensile strength of friction stir welded AA 2219 aluminium alloy. They used the Hooke and Jeeves algorithm to optimize the FSW parameters to achieve highest tensile strength in the joints. Furthermore, Heidarzadeh et al. [20, 21] have predicted the mechanical properties of the friction stir welded pure copper plates with different thicknesses of 2 and 5 mm. They have developed the statistical models to predict and optimize the mechanical properties of the joints using Design Expert software.

Table 1 Coded and actual values of FSW parameters

Parameters	Unit	Levels				
		−1.68	−1	0	1	1.68
Rotational speed	rpm	664	800	1,000	1,200	1,336
Traverse speed	mm/min	58	75	100	125	142
Axial force	kN	5.32	6	7	8	8.68

Table 2 Design layout including experimental and predicted values

No.	Run	Coded values of parameters			Mechanical properties			
		(A)	(B)	(C)	UTS(MPa)		%EL	
					Experimental	Predicted	Experimental	Predicted
1	5	−1	−1	−1	227	230.27	4.6	4.48
2	9	1	−1	−1	276	273.22	7.9	8.00
3	1	−1	1	−1	232	228.51	4.1	4.05
4	13	1	1	−1	259	262.46	7.4	7.27
5	10	−1	−1	1	268	264.66	4.8	5.04
6	4	1	−1	1	271	274.62	7.9	8.06
7	12	−1	1	1	259	261.90	4.8	4.81
8	3	1	1	1	266	262.85	7.3	7.53
9	21	−1.68	0	0	229	229.45	4.2	4.20
10	19	1.68	0	0	267	266.37	9.6	9.44
11	6	0	−1.68	0	257	256.60	6.3	6.13
12	25	0	1.68	0	245	245.22	5.3	5.32
13	14	0	0	−1.68	267	266.79	5.4	5.58
14	23	0	0	1.68	296	296.04	6.6	6.27
15	17	0	0	0	302	305.67	6.3	6.17
16	20	0	0	0	305	305.67	6.1	6.17
17	18	0	0	0	306	305.67	6.5	6.17
18	11	0	0	0	305	305.67	6.1	6.17
19	8	0	0	0	307	305.67	6.1	6.17
20	15	0	0	0	309	305.67	5.9	6.17

Table 3 Chemical composition of the BM

AL	Ti	Zn	Cu	Cr	Fe	Mn	Si	Mg
85.44	0.08	4.70	0.10	0.14	0.35	0.24	0.30	1.30

Special characteristics of aluminum alloys have made it a good candidate for replacing the steel structures in marine industry. The 5xxx aluminum alloys possess better corrosion resistance (especially in seawater and marine performances) compared to the other series of aluminum alloys. An alternative to 5xxx alloys could be the 7xxx (Al–Zn–Mg) alloys due to their better mechanical properties. Despite good weldability of these types of alloys, conventional fusion welding methods reduce their mechanical and corrosion properties. An excellent alternative to the conventional fusion welding methods can be the FSW process.

Even though the prior investigators [9, 19] explored mathematical models in the case of some aluminium alloys, a research into establishing mathematical relationships between the FSW parameters and mechanical properties of friction stir welded AA 7020 aluminium alloy joints is lacking. Therefore, the aim of this study was to apply RSM in conjunction with central composite rotatable design (CCRD), to establish the functional relationships between FSW parameters i.e. rotational speed, traverse speed and tool axial force, and responses of UTS and tensile elongation (EL) of friction stir welded AA 7020 alloy joints.

2 Materials and Methods

2.1 Design of Experiments

In this investigation, CCRD was used for design of experiments because it needs fewer experiments than the full and partial factorial design. For this purpose, CCRD including 20 runs, three

FSW parameters [rotational speed (A), traverse speed (B) and axial force (c)] and five levels ($\pm \beta, \pm 1, 0$) was employed to design of experiments, in which $\beta = 2^{k/4} = 2^{3/4} \approx 1.68$ and k is number of independent parameters [9]. The levels and actual values of FSW parameter are shown in Table 1. In addition, the evaluated and measured responses were the UTS and EL. Moreover, Design-Expert Version 8.0 software was used for preparing the experimental design which is presented in Table 2.

2.2 FSW of the joints and experimental details

The AA 7020 aluminium alloy plates of 4 mm thickness with UTS of 410 MPa and EL of 13 % were utilized as

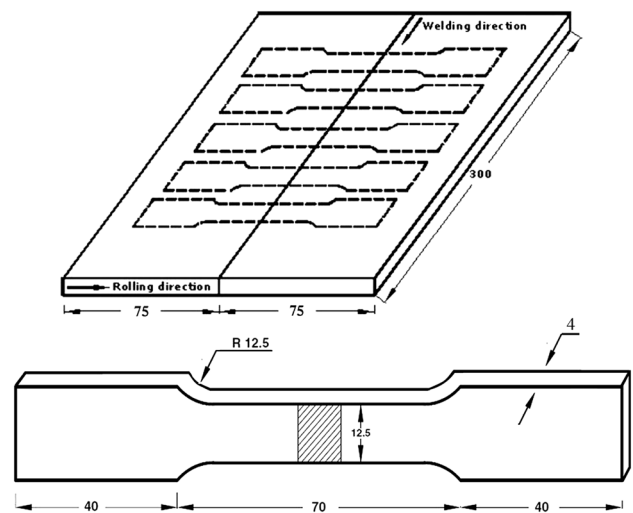


Fig. 2 Location in the joint and schematic illustration of tensile test

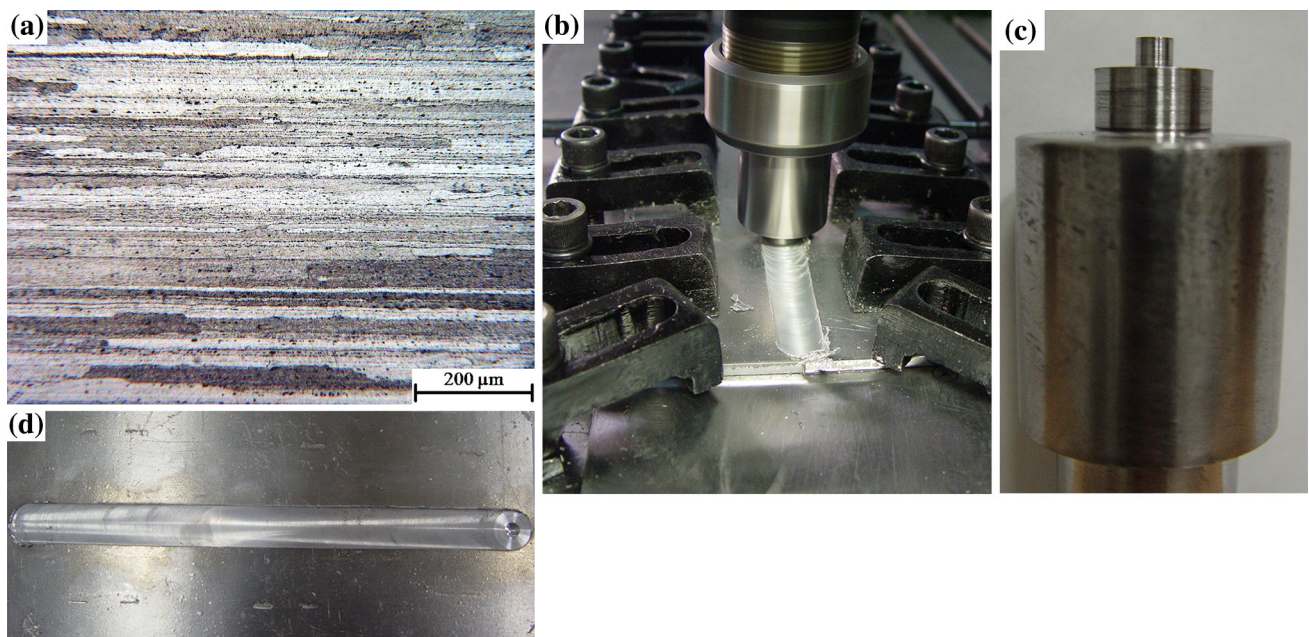


Fig. 1 a Microstructure of the BM, b designed fixtures, c tool pin profile and d defect free joint

base metal (BM). The chemical composition and microstructure of the BM are presented in Table 3, and Fig. 1a, respectively. The plates were clamped in place by fixtures as illustrated in Fig. 1b. A FSW tool made of H13 steel with a shoulder (12 mm diameter) and a simple cylindrical pin (4 mm diameter and 3.7 mm length) was used, as shown in Fig. 1c, and the tilt angle of the tool relative to the work piece was set at 2.5.

FSW perpendicular to the rolling direction of plates was done to fabricate the joints. A lot of FSW were processed to find the limitation of each FSW parameter (levels ± 1 in Table 1) by altering one of them and keeping the rest of them at constant amounts. Reasonable limits of the parameters were selected in such a way that the joint should be free from observable defects as presented in Fig. 1d. Consequently, the joints were produced according to the experimental design layout i.e. Table 2. The microstructures of the joints were analyzed using an optical microscope (OM). Accordingly, the metallographic specimens

were cut from the joints transverse to the welding direction, then polished and etched with Keller's reagent (95 mL water, 2.5 mL HNO₃, 1.5 mL HCl, 1.0 mL HF). In addition, the tensile strength and elongation of the joints were measured by tensile test. For this purpose, five tensile specimens were prepared per joint (Fig. 2) according to the ASTM: E8 M standard and tensile tests were conducted at a cross head speed of 1 mm/min. Moreover, the fractography of the tensile specimens were done using scanning electron microscope (SEM).

2.3 Establishing Mathematical Model

The mathematical models were established using a second order polynomial regression model including the main and interaction influences of the FSW parameters. If the measured responses (Y) i.e. UTS and EL of the joints are a function of FSW parameters i.e. rotational speed (A), traverse speed (B) and axial force (C), the response surface

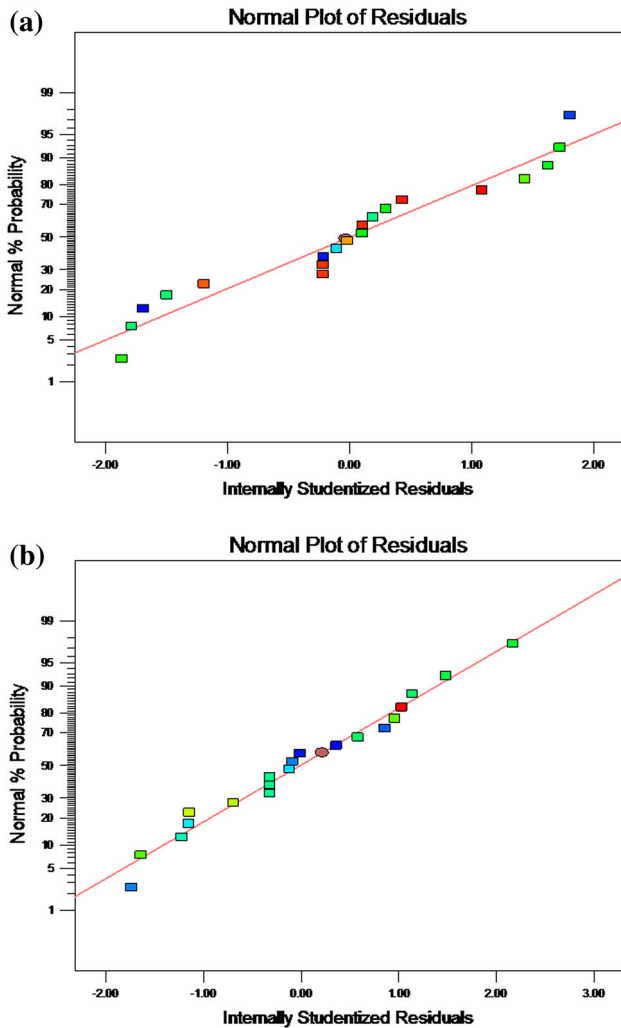


Fig. 3 Normal probability plot of residuals for: a UTS, and b EL

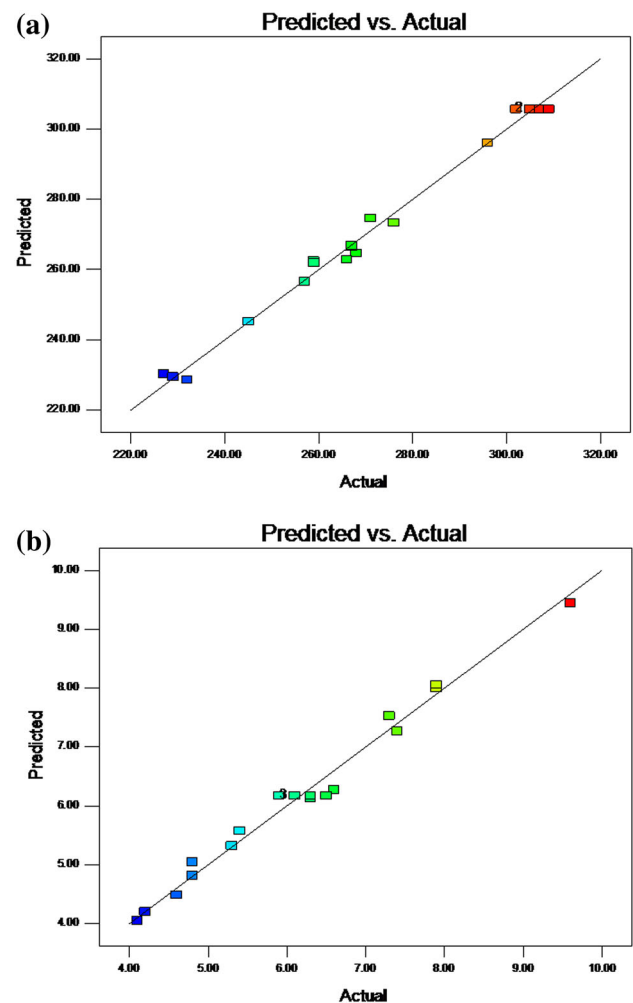


Fig. 4 Predicted versus actual response plot for: a UTS, and b EL

can be explored as Eq. 1. As well, the employed regression equation in this study is presented as Eq. 2:

$$Y = f(A, B, C) \tag{1}$$

$$Y = b_0 + \sum_{i=1}^k b_i X_i + \sum_{i=1}^k b_{ii} X_i^2 + \sum_{i < j} b_{ij} X_i X_j \tag{2}$$

In Eqs. 1 and 2, Y is the measured responses, X_i and X_j are the independent variables, b₀ stand for the mean value of responses and b_i, b_{ii} and b_{ij} are linear, quadratic and interaction constant coefficients, correspondingly. In addition, the coefficients of the Eq. 2 can be computed using the Eqs. 3–6 [11, 22–24]:

$$b_0 = 0.142857 \left(\sum Y \right) - 0.035714 \sum \sum (X_{ii} Y) \tag{3}$$

$$b_i = 0.041667 \left(\sum X_i Y \right) \tag{4}$$

$$b_{ii} = 0.03125 \sum (X_{ii} Y) + 0.00372 \sum \sum (X_{ii} Y) - 0.035714 \left(\sum Y \right) \tag{5}$$

$$b_{ij} = 0.0625 \sum (X_{ij} Y) \tag{6}$$

The selected polynomials considering the three FSW parameters (A, B and C) will be presented as Eq. 7. Furthermore, the Design-Expert software at 95 % confidence level was employed in order to compute the coefficients of the models. Moreover, the sufficiency of the models was confirmed using ANOVA, and models were illustrated by contour and 3D plots.

$$Y = b_0 + b_1(A) + b_2(B) + b_3(C) + b_{11}(A^2) + b_{22}(B^2) + b_{33}(C^2) + b_{12}(AB) + b_{13}(AC) + b_{23}(BC) \tag{7}$$

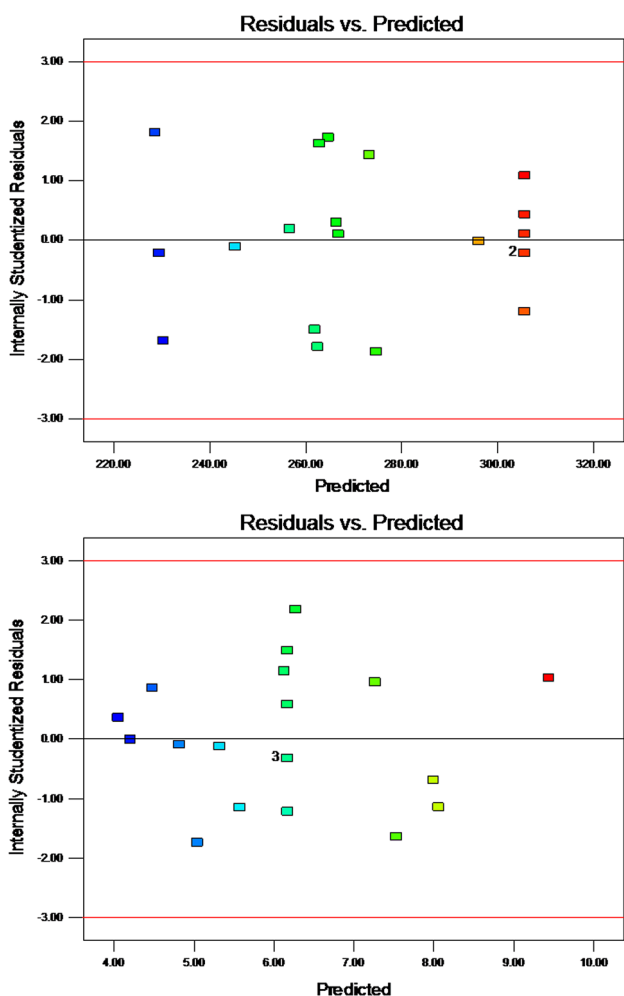


Fig. 5 Residuals versus the predicted response plot for: a UTS, and b EL

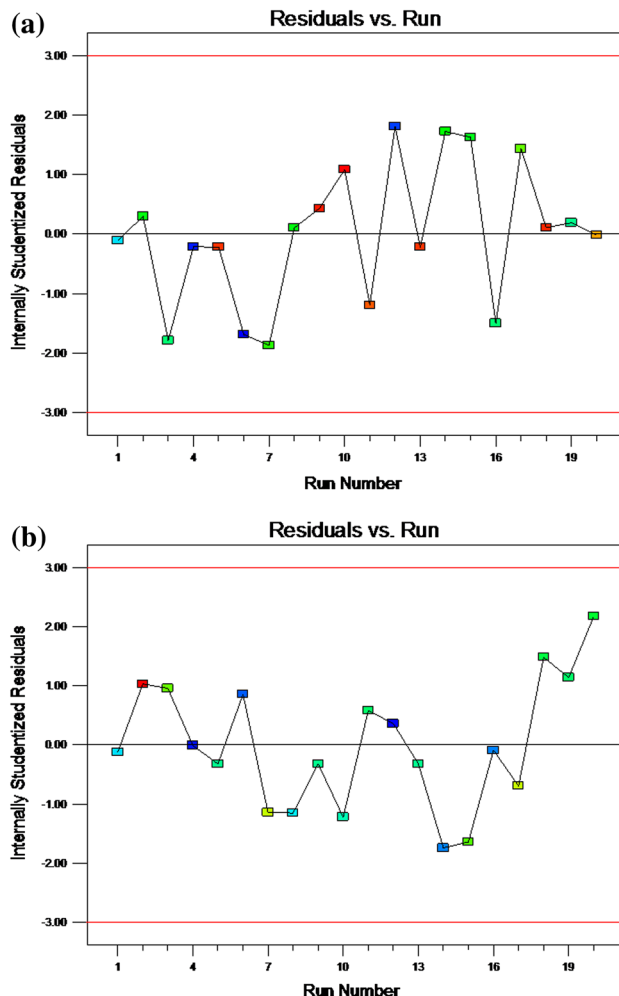


Fig. 6 Residuals versus the experimental run plot for: a UTS, and b EL

Table 4 ANOVA table for response UTS

Source	Sum of squares	Degree of freedom	Mean square	F value	P value	
Model	14,167.26	9	1,574.14	138.94	<0.0001	Significant
A	1,645.51	1	1,645.51	145.24	<0.0001	
B	156.17	1	156.17	13.78	0.0040	
C	1,032.95	1	1,032.95	91.17	<0.0001	
AB	40.50	1	40.50	3.57	0.0880	
AC	544.50	1	544.50	48.06	<0.0001	
BC	0.50	1	0.50	0.044	0.8378	
A ²	6,009.93	1	6,009.93	530.47	<0.0001	
B ²	5,401.85	1	5,401.85	476.80	<0.0001	
C ²	1,060.23	1	1,060.23	93.58	<0.0001	
Residual	113.29	10	11.33			
Lack of fit	85.96	5	17.19	3.14	0.1151	Not significant
Pure error	27.33	5	5.47			
R ²	0.9921					
Adjusted R ²	0.9849					

Table 5 ANOVA table for response EL

Source	Sum of squares	Degree of freedom	Mean square	F value	P value	
Model	36.10	9	4.01	68.00	<0.0001	Significant
A	33.16	1	33.16	562.21	<0.0001	
B	0.79	1	0.79	13.37	0.0044	
C	0.58	1	0.58	9.86	0.0105	
AB	0.045	1	0.045	0.76	0.4029	
AC	0.12	1	0.12	2.12	0.1761	
BC	0.020	1	0.020	0.34	0.5733	
A ²	0.76	1	0.76	12.96	0.0049	
B ²	0.36	1	0.36	6.15	0.0326	
C ²	0.11	1	0.11	1.89	0.1994	
Residual	0.59	10	0.059			
Lack of fit	0.38	5	0.075	1.77	0.2740	Not significant
Pure error	0.21	5	0.043			
R ²	0.9839					
Adjusted R ²	0.9695					

3 Results and Discussion

3.1 Numerical Relationships and ANOVA Analysis

The numerical relationships between the FSW parameters and the responses UTS and EL have been achieved as follows:

$$\begin{aligned}
 UTS = & 305.67 + 10.98A - 3.38B + 8.70C - 2.25AB \\
 & - 8.25AC - 0.25BC - 20.42A^2 - 19.36B^2 \\
 & - 8.58C^2
 \end{aligned} \quad (8)$$

$$\begin{aligned}
 EL = & 6.17 + 1.56A - 0.24B + 0.21C - 0.075AB \\
 & - 0.12AC + 0.05BC + 0.23A^2 - 0.16B^2 - 0.088C^2
 \end{aligned} \quad (9)$$

The Eqs. 8 and 9 predict the UTS and EL of the friction stir welded AA 7020 aluminium alloy joints. The normal

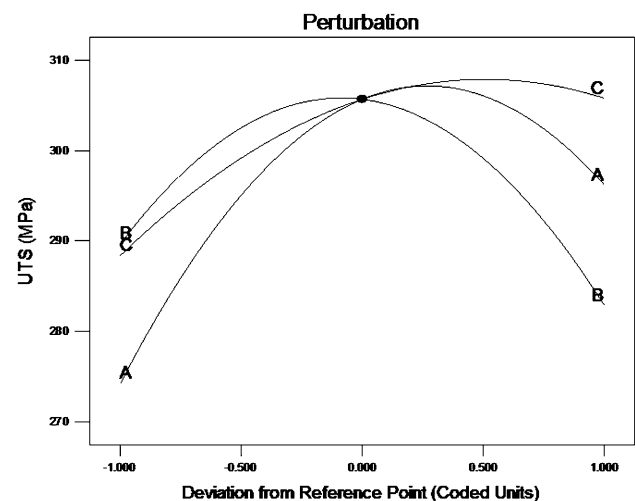


Fig. 7 Perturbation plot illustrating the influence of FSW parameters on the UTS

plot of residuals, the predicted versus actual response plot, the residuals versus the predicted response plot, and the residuals versus the experimental run plot are respectively illustrated in Figs. 3, 4, 5 and 6, for UTS and El. The

normal probability plot indicates whether the residuals follow a normal distribution, in which case the points will follow a straight line. Figure 3 demonstrates that errors are extended normally because the residuals follow a straight

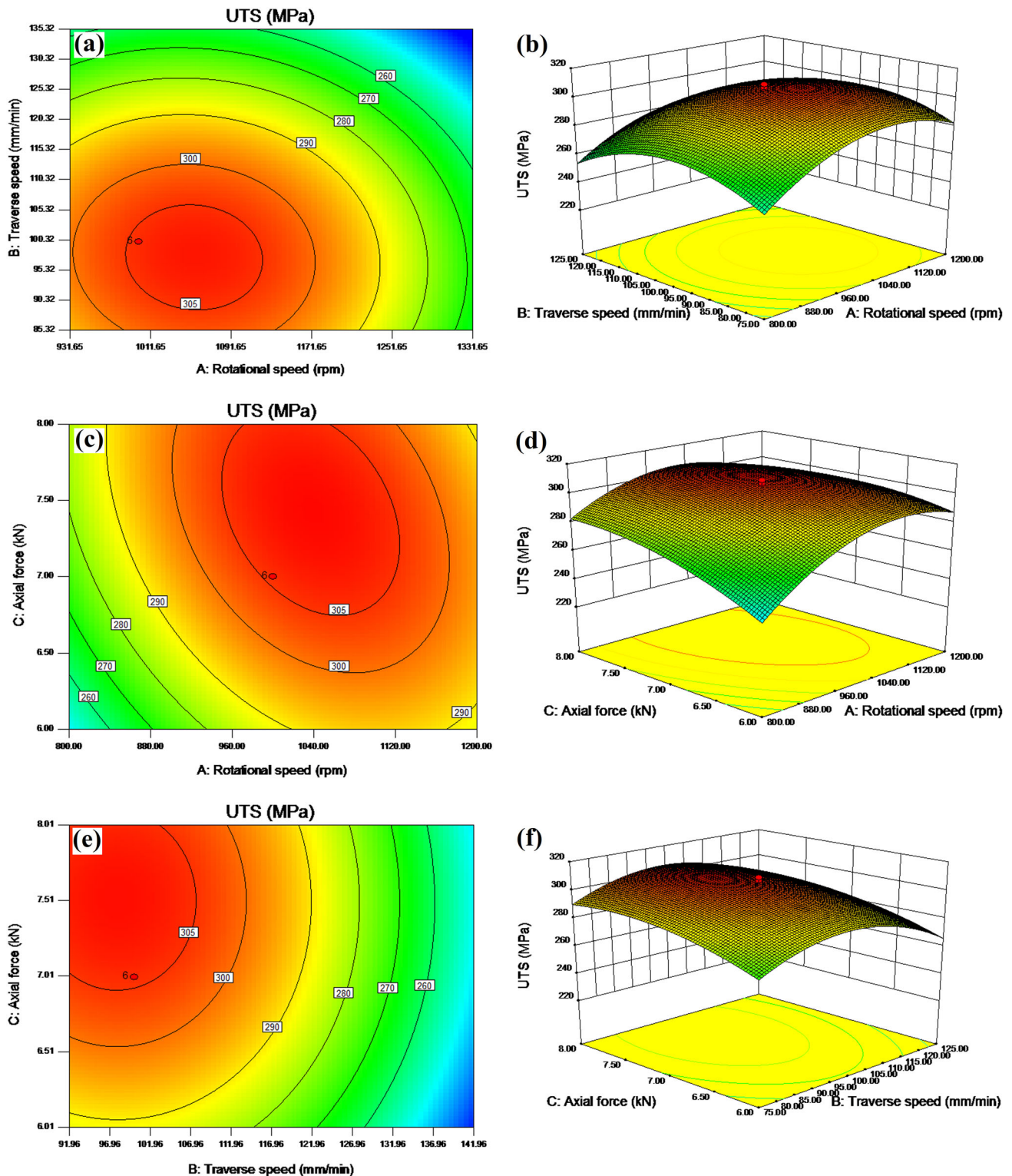


Fig. 8 Contour and 3D plots for the response UTS

line. Figure 4 reveals that the predicted responses values are in good agreement with the actual ones within the ranges of the FSW process parameters, because the data points are split evenly by the 45 degree line. Figures 5 and 6 reveal that numerical models predict the responses adequately due to randomly scattered residuals.

The ANOVA analysis results for the responses UTS and EL are summarized in Tables 4 and 5. The F value, P value, R^2 and adjusted R^2 are used for identifying the more significant model and coefficients. Larger F value, R^2 and adjusted R^2 , and smaller P value reveal that the model or a coefficient is significant. According to the Tables 4 and 5, the F value, P value, R^2 and adjusted R^2 for the predicted UTS and EL models are 68.00, <0.0001, 0.9839, 0.9695, and 138.94, <0.0001, 0.9921, 0.9849, respectively. Therefore, the predicted models are very adequate and significant.

Additionally, P values <0.05 verify that the coefficients are significant and P values >0.1 mean that the coefficients are not significant. Thus, according to the P-values, A, B,

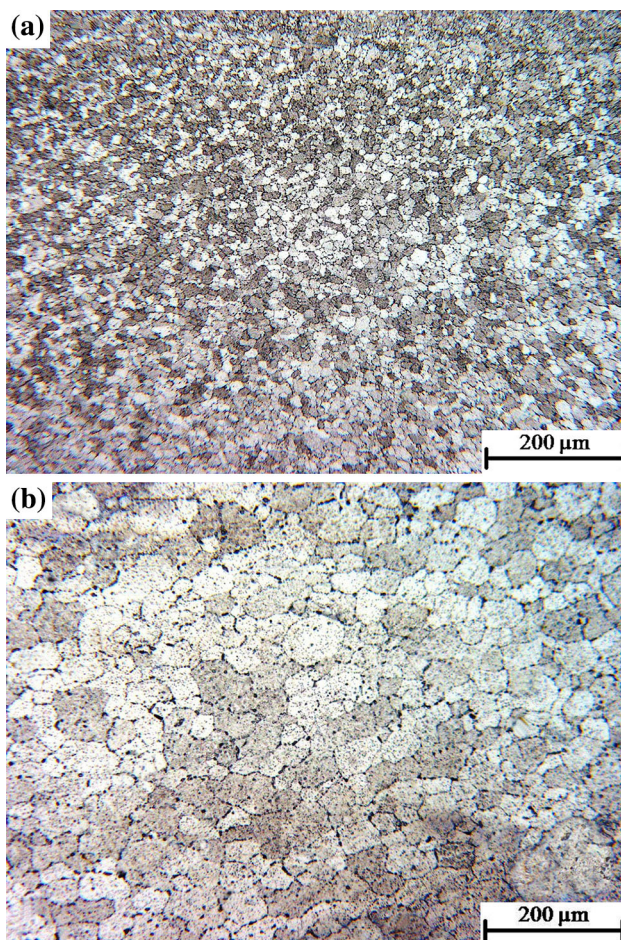


Fig. 9 Microstructures of joints in: **a** Low heat input condition, and **b** high input condition

C, AC, A^2 , B^2 and C^2 are significant terms for predicted UTS model. Similarly, A, B, C, A^2 and B^2 are significant terms for EL model. After reduction of the models by considering only the significant terms, the following mathematical models are achieved:

$$UTS = 305.67 + 10.98A - 3.38B + 8.70C - 8.25AC - 20.42A^2 - 19.36B^2 - 8.58C^2 \quad (10)$$

$$El = 6.17 + 1.56A - 0.24B + 0.21C + 0.23A^2 - 0.16B^2 \quad (11)$$

Furthermore, the F values prove that the order of the more significant terms in UTS and EL models are as follows, respectively: $A^2 > B^2 > A > C^2 > C > AC > A^2$, $A > A^2 > B > C > B^2$.

3.2 Effect of FSW Parameters on UTS

The perturbation plot for UTS of the joints is presented in Fig. 7. Also, Fig. 8a–f show the contour and 3D surface plots. These plots illustrate the interaction effect of any two FSW parameters on the UTS when the other parameter is on its level zero (center level). Figures 7 and 8a–f reveal that increase in rotational speed, traverse speed and axial force cause an increase in UTS of the joints up to a maximum value, and then decrease. The lower rotational speeds, higher traverse speeds and lower axial forces create insufficient heat and deformation, which bring about poor plastic flow and defect generation in the joints, and hence lower UTS.

The higher rotational speeds, lower traverse speeds and higher axial forces result in sound welds, but produce

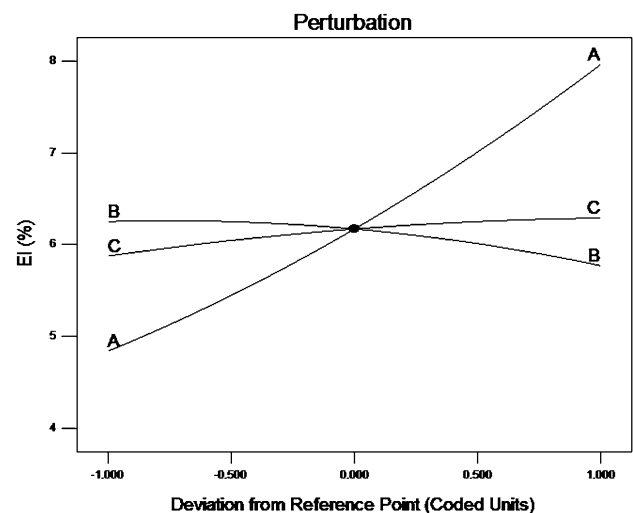


Fig. 10 Perturbation plot illustrating the influence of FSW parameters on the EL

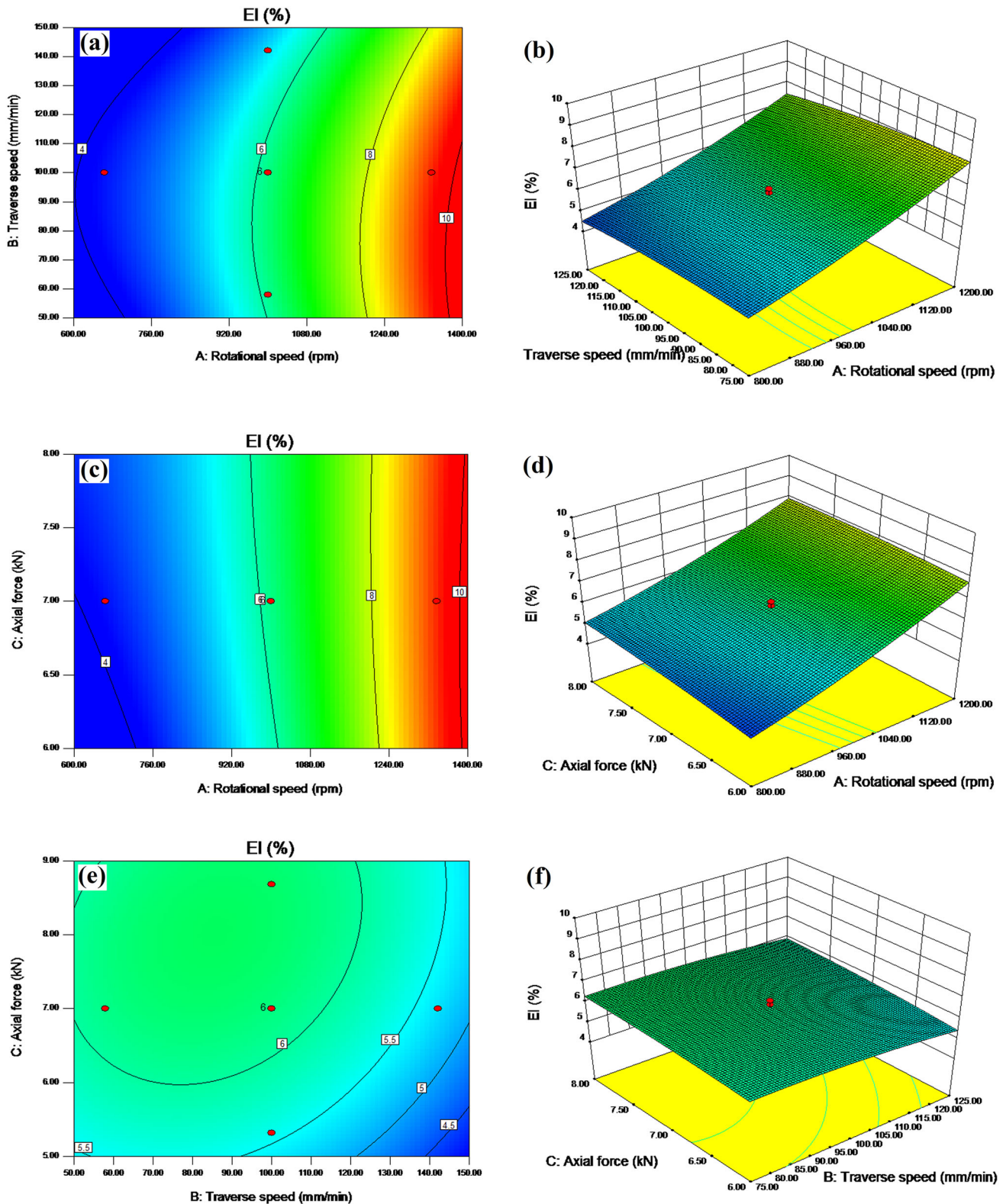


Fig. 11 Contour and 3D plots for the response EI

enough heat for some metallurgical phenomena like grain growth [9], solubilization and coarsening of strengthening precipitates in the joints [8], and reduction of dislocation

density [20, 21] which decrease the UTS of the joints. The microstructures of the joints welded at both low and high heat input conditions are shown in Fig. 9, which expose

that in low heat input condition the grain of the joint is smaller than that of the high heat input condition. According to the classical Hall–Petch relationship, the fine and coarse grains cause higher and lower UTS values, correspondingly.

3.3 Effect of FSW Process Parameters on EL

The perturbation, counter and 3D surface plots for the EL of the joints are shown in Figs. 10 and 11a–f. An increase in rotational speed and axial force, and a decrease in traverse speed cause higher EL, continuously. Higher heat input conditions (i.e. higher rotational speed, higher axial force and lower traverse speed) results in sufficient plastic deformation [21] and elimination of the defects in the joints, and hence higher EL. As well, higher heat input conditions lead to metallurgical transformations such as grain coarsening, growth of precipitates and lowering of dislocation density [17–21]. According to Fig. 9a–b, higher heat input conditions result in bigger grain sizes in the SZ of the joint, which does not agree with higher EL. Therefore, the higher elongation of the joints at higher heat input conditions could be related to other phenomena like coarsening of the secondary phase particles and lower dislocation densities in the SZ [20, 21]. According to the Fig. 12, the fracture surfaces of the joints are composed of deep dimples, shallow dimples, sheared dimples and cleavage facets. Aluminium alloys with face centered cubic (FCC) crystallographic structure are normally considered to fracture through ductile mechanism and not cleavage due to their several active slip systems. However, cleavage mechanism can take place for FCC materials under particular conditions. As mentioned before, there are some characteristics in the fracture surfaces of friction stir welded specimens which show both the ductile and cleavage fracture mechanisms. The expression ‘quasi-cleavage’ is frequently employed to explain this type of fracture mechanism, and it is a localized, regularly separated characteristic on a fracture surface that reveals features of both cleavage and plastic deformation [26]. Likewise, fractography of the joints confirm the higher EL of the joints welded at higher heat input conditions (Fig. 12a, b). Fracture surface of the joints welded at higher heat input condition (Fig. 12b) has more dimples and fewer facets than that of the joints welded at lower heat input condition (Fig. 12a). Accordingly, higher heat input conditions reveal more ductility which verifies higher EL of the joints.

3.4 Optimization of FSW Parameters

The optimum FSW parameters were measured using contour and 3D plots in which the UTS and EL of the joints were maximized. Accordingly, the results show that the

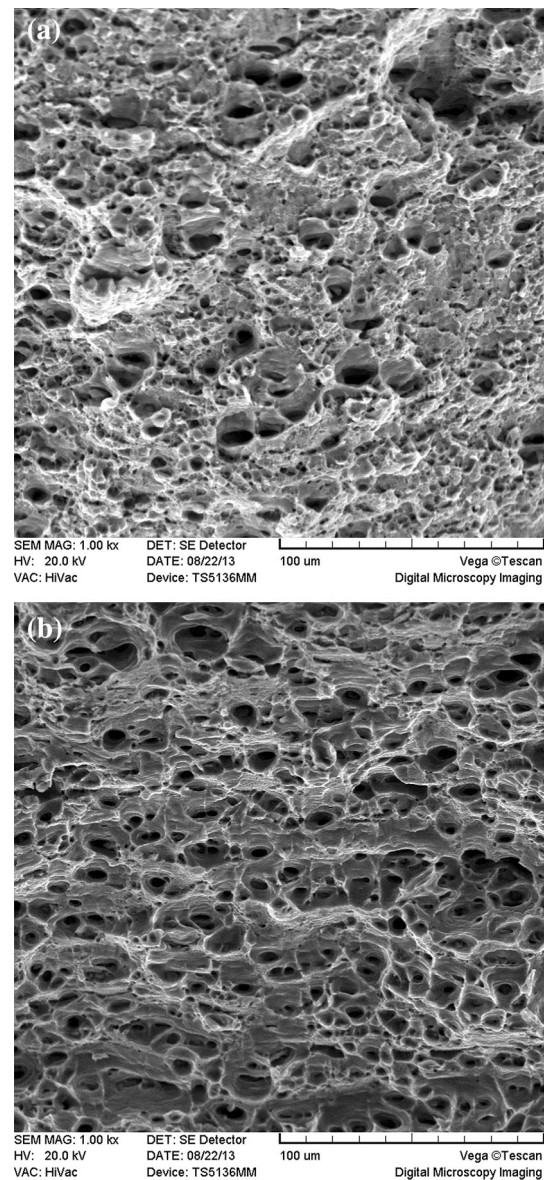


Fig. 12 SEM fractographs of tensile specimens welded at: **a** Lower heat input condition, and **b** higher input condition

Table 6 The optimum FSW condition for maximizing the UTS and EL

Measured response	Optimum rotational speed (rpm)	Optimum traverse speed (mm/min)	Optimum axial force (kN)
UTS	1,055	97	7.4
EL	1,320	72	7

maximum values of the UTS and EL for the joints that can be achieved during FSW of AA 7020 alloy are 308.5 MPa and 9.4 %, relatively. In addition, the optimum FSW parameters for maximizing the UTS and EL of the joints were calculated as summarized in Table 6.

4 Conclusions

- (1) The range of FSW parameters to produce defect free joints of AA 7020 aluminum alloy was achieved.
- (2) Numerical models were effectively established to predict and optimize the UTS and EL of AA 7020 joints using RSM based on a central composite rotatable design. Also, the ANOVA analysis revealed that the models can be successfully applied for prediction of tensile properties of the joints.
- (3) With increasing heat input during FSW i.e. higher rotational speed, lower traverse speed and higher axial force, UTS of the AA 7020 joints increased up to a maximum amount, and then decreased.
- (4) Higher rotational speeds and axial forces, and lower traverse speeds resulted in higher EL of the joints, continuously. Moreover, the fractography of the joints confirmed that the joints welded at higher heat input conditions resulted in more ductile fracture mode than that of the joints welded at lower heat input conditions.
- (5) The highest values of 308.5 MPa and 9.4 % respectively for the UTS and EL of the joints can be obtained during FSW of AA 7020 alloy. Furthermore, the optimized rotational speed, traverse speed and axial force to get maximum amounts of UTS and EL were 1,055 rpm–97 mm/min–7.4 kN and 1,320 rpm–72 mm/min–7 kN correspondingly.

References

1. Marzbanrad J, Akbari M, Asadi P, and Safaee S, *Metall Mater Trans B* **45** (2014) 1887.
2. Tutunchilar S, Givi M K B, Haghpanahi M, and Asadi P, *Mater Sci Eng A* **534** (2012) 557.
3. Salekrostam R, Givi M K B, Asadi P, and Bahemmat P, *Defect Diffus Forum* **297-301** (2010) 221.
4. Heidarzadeh A, Jabbari M, and Esmaily M, *Int J Adv Manuf Tech* (in press).
5. Farrokhi H, Heidarzadeh A, and Saeid T, *Sci Technol Weld Joi*, **18** (2013) 697.
6. Motallebnejad P, Saeid T, Heidarzadeh A, Darzi Kh, and Ashjari M, *J Mater Des* **59** (2014) 221.
7. Box E P, and Hunter J S, *Annals Math Stat* **28** (1957) 195.
8. Heidarzadeh A, Khodaverdizade H, Mahmoudi A, and Nazari E, *J Mater Des* **37** (2012) 166.
9. Rajakumar S, Muralidharan C, and Balasubramanian V, *T Non-ferr Metal Soc* **20** (2010) 1863.
10. Rajakumar S, Muralidharan C, and Balasubramanian V, *J Mater Des* **32** (2011) 2878.
11. Ilkhchi A R, Soufi R, Hussain G, Barenji R V, and Heidarzadeh A, *Metall Mater Trans B* (in press).
12. Jayaraman M, Sivasubramanian R, Balasubramanian V, and Lakshminarayanan A K, *J Manuf Sci Prod Res* **9** (2008) 1.
13. Lakshminarayanan A K, and Balasubramanian V, *Trans Non-ferrous Met Soc China* **18** (2007) 548.
14. Lakshminarayanan A K, and Balasubramanian V, *Trans Non-ferrous Met Soc China* **19** (2009) 9.
15. Elangovan K, Balasubramanian V, and Babu S, *Mater Des* **30** (2009) 188.
16. Babu S, Elangovan K, Balasubramanian V, and Balasubramanian M, *Met Mater Int* **15** (2009) 321.
17. Karthikeyan R, and Balasubramanian V, *Int J Adv Manuf Tech* **51** (2010) 173.
18. Rajakumar S, Muralidharan C, and Balasubramanian V, *Trans Nonferrous Met Soc China* **20** (2010) 1863.
19. Rajakumar S, and Balasubramanian V, *J Mater Des* **40** (2012) 17.
20. Heidarzadeh A, Saeid T, Khodaverdizadeh H, Mahmoudi A, and Nazari E, *Metall Mater Trans B* **44B** (2013) 175.
21. Heidarzadeh A, and Saeid T, *J Mater Des* **52** (2013) 1077.
22. Azadbeh M, Mohammadzadeh A, and Danninger M, *J Mater Des* **55** (2014) 633.
23. Mohammadzadeh A, Azadbeh M, and Danninger M, *Powder Metall* (in press).
24. Mohammadzadeh A, Azadbeh M, and Namini A S, *Sci Sinter* **46** (2014) 23.
25. Yia S, Sua Y, Qia B, Sua Z, and Wana Y, *Sep Purif Technol* **71** (2010) 252.
26. ASM Handbook, volume 12: fractography. ASM International Materials Park (1987) 55.